Impact of altimeter-buoy data pairing methods on the validation of Sentinel-3A coastal significant wave heights

Guillaume Dodet[a], Grégoire Mureau[b], Mickaël Accensi[a], Jean-François Piollé[a]

[a] *Univ Brest, Ifremer, CNRS, IRD, LOPS, Plouzané, F-29280, France*
[b] *Ifremer, IRSI, ISI Service Ingénierie des Systèmes d'Information, Plouzané, F-29280, France*

Abstract

Sea state information is critical for a broad range of human activities (e.g. shipping, marine energy, marine engineering) most of them being concentrated along the coastal zone. Satellite altimeter records of significant wave heights represent the largest source of sea state observations available to date. However, the quality of altimeter observations is downgraded in the coastal zone due to surface heterogeneity within the radar signal footprint. In the last decades, increasing efforts have been devoted to exploit altimeter observations closer to the coast, using new sensor technologies (e.g. Ka-band or Delay-Doppler radar altimeters), dedicated waveform retracking algorithms or post processing filtering techniques. One major difficulty that remains to assess the performance of coastal altimetry in the coastal zone is the reduced number of valid altimeter records and the increased sea state variability, which requires the development of new methods to pair and compare nearby altimeter and buoy data. In this study, we use a high-resolution numerical wave model implemented over the European coastal waters in order to characterize the spatial variability of sea states in the proximity of coastal in situ buoys. Areas of sea state similarity are defined from the computation of systematic and random errors between the time series simulated at the station and those of neighboring nodes. These areas are then used to compute buoy – altimeter matchup statistics and estimate altimeter errors with respect to the buoy data. Additional methods, based on the dynamic comparison between model results at the buoy location and at the altimeter ground measurement are also investigated. These different methods are used to assess the quality of Sentinel-3A 20Hz significant wave height acquisitions in both offshore and coastal waters. Three Sentinel-3A data flavours are compared: the pseudo low resolution mode acquisitions,the SAR mode acquisitions and the Low Resolution with Range Migration Correction (LR-RMC) acquisitions. Comparisons against in situ and high resolution model clearly demonstrate the improved performance of the SAR and LR-RMC data relative to PLRM data. In particular, the LR-RMC processing is shown to provide consistent SWH records within the 0-20km coastal strip (and as close as 1km from the coast), with average normalized bias = 2.4%, scatter index = 18.9% and correlation coefficient = 0.95.

Keywords:

1. Introduction

Collecting long-term, frequent and accurate coastal sea state information is critical for a broad range of human activities, such as commercial shipping, harbour operations, marine and coastal engineering, or marine energy resource assessment (Ardhuin et al., 2019). In the current context of accelerating sea level rise, coastal sea state information is also required to better understand and predict sea level changes along the coasts. Indeed, wave-induced nearshore processes cause significant fluctuations of the sea level at the shoreline, for instance due to wave setup, infragravity waves, or swash zone excursion (Dodet et al., 2019b), that can dominate the extreme total water level signal along many exposed coastlines (Serafin et al., 2017). Moreover, sea states are known to modify the scattering properties of the sea surface, with higher reflectivity in the wave troughs than in the wave crests, resulting in an underestimation of the mean sea level of the order of a few percents of the significant wave height (SWH) (Yaplee et al., 1971; Jackson, 1979). This so-called sea state bias still represents one of the major source of errors in satellite altimeter range corrections in the coastal zone (Vignudelli et al., 2019).

Satellite altimeter records of SWH represent the largest source of sea state observations available to date. However, the quality of altimeter acquisitions is degraded in the coastal zone due to land contamination and sea surface heterogeneities within the radar signal footprint (Vignudelli et al., 2019). Over the last decades, increasing efforts have been devoted to exploit altimeter observations closer to the coast using new sensor technologies (e.g. Ka-band and synthetic aperture radar altimeters), improved waveform retracking algorithms (e.g. Passaro et al., 2018; Tourain et al., 2021) or post processing filtering techniques (e.g. Quilfen and Chapron, 2020). Among these recent innovations, synthetic aperture radar (SAR) altimetry (also known as Delay-Doppler altimetry) appears particularly promising for monitoring the coastal zone, thanks to a finer along-track-resolution and a lower noise level (Raney, 1998). In this study, we investigate the performance of the SAR Radar Altimeter (SRAL) instrument on-board the Copernicus Sentinel-3A mission, to retrieve significant wave heights in the coastal zone. In particular, different mode of acquisitions permitted by this instrument, described in the next Section, will be compared.

A number of studies have explored the performance of altimeter missions for measuring wave heights in the coastal zone based on comparisons with in situ measurements (e.g. Hithin et al., 2015; Nencioli and Quartly, 2019; Jiang et al., 2022) and high resolution numerical wave models (Schlembach et al., 2020; Alday et al., 2022). Two major difficulties have been identified for the interpretation of coastal altimeter validation results. On one hand, the number of invalid data drastically increases close to the coast so that improved performance are often obtained at the expense of a reduced sample size resulting from a highly selective data editing (Schlembach et al., 2020), which is not systematically documented. On the other hand, the representativeness error due to the spatial and temporal separation distances between pairs of altimeter and in situ measurements strongly increases in the coastal zone and customary collocation method based on fixed thresholds (usually 50km and 30min) are no longer valid. To overcome these limitations, several authors developed data pairing methods for the coastal zone based on numerical wave model results. Nencioli and Quartly (2019) used wave model hindcast results around coastal UK wave buoys in order to define high correlation areas between buoy and surrounding nodes. The selection of altimeter data to be compared with the buoy data is then based on these high correlation areas, so that spatial representativeness error is reduced. Jiang et al. (2022) revisited this experiment and proposed a dynamic correction to the buoy measurements based on wave model outputs in order to account for SWH variability without reducing the number of altimeter-buoy matchups.

In this study we use a high-resolution numerical wave model implemented over the European coastal waters in order to characterize the spatial variability of sea states in the proximity of coastal in situ buoys. Buoy representativeness areas are defined from the computation of systematic and random errors between the time series simulated at the station and those of neighboring nodes. These areas are then used to compute buoy – altimeter matchup statistics and estimate altimeter errors with respect to the buoy data. Additional methods considered in this study are based on the dynamic comparison between model results at the buoy location and at the altimeter ground measurement, to ensure that (modelled) spatial variability is low before comparing altimeter and in situ data. These different methods are used to assess the quality of Sentinel-3A 20Hz SWH acquisitions in both pseudo low resolution and SAR modes. For this latter mode, two processing methods (SAR and LR-RMC) are compared. The Sentinel-3A and buoy datasets as well as the different data pairing methods considered in this study are presented in the next section. Then comparisons of the different methods and the impact on Sentinel-3A coastal validation are presented in Section 4. Finally the results are discussed and summarized in Section 5.

2. Datasets

2.1. Sentinel-3A

The Copernicus Sentinel-3A (S3A hereafter) mission, launched in February 2016, is a low Earth polar orbiting satellite operating at an average altitude of 815 km above the Earth surface with a repeat cycle of 27 days. It carries onboard a SAR Radar Altimeter (SRAL), which provides high-resolution SWH measurements. The SAR processing mode was first developed for the European Space Agency (ESA) mission Cryosat for its measurements over ice (and later extended to small sample regions of the ocean), but S3A is the first altimeter mission to operate in this mode globally over all surfaces. SAR altimeters present a narrow ($\sim 250m$) footprint in the along-track direction independent of the sea state conditions, which present a major advantage in comparison to conventional low resolution mode altimetry for which the diameter of the altimeter footprint can exceeds 10km during rough sea state conditions (Chelton et al., 1989). This narrow-band footprint results from the exploitation of radar pulses transmitted at very high rate (ten times as high as for LRM), and for which pulse-to-pulse coherency and Doppler information are used to localize radar echoes and form multi-looked waveforms (Raney, 1998). Despite its clear advantages in terms of resolution and noise level (Boy et al., 2017), SAR processing has also proven to be particularly sensitive to the presence of swells for retrieving accurate wave height information (Moreau et al., 2018). To overcome this issue, Moreau et al. (2021) implemented the Low Resolution with Range Migration Correction (LR-RMC hereafter) method, which uses an alternative and less complex averaging (stacking) operation so that all the Doppler beams produced in a radar cycle (4 bursts of 64 beams for the S3 open-burst mode) are incoherently combined to form a multi-beam echo. Contrarily to the narrow-band SAR technique, the LR-RMC processing enlarges the effective footprint to average out the effects of surface waves that are known to impact SAR-mode performances. On the other hand, the number of averaged beams is as high as in current SAR-mode processing, thus providing a noise reduction at least equally good.

The S3A measurements considered in this study are along-track SWH records at 20Hz posting rate (corresponding to approximately 300m spacing between two records) from three different datasets, namely the Pseudo Low Resolution (PLRM), SAR and LR-RMC datasets. The PLRM and SAR data are both from the EUMETSAT SRAL/MWR L2 Marine products (https://www.eumetsat.int/sentinel-3), while the LR-RMC data are from the ESA Sea State Climate Change Initiative project (https://climate.esa.int/en/projects/sea-state/). For each dataset, data editing was performed based on the available surface type and quality flag information.

2.2. Wave buoys

The CMEMS In Situ Thematic Assembly Center (CMEMS INSTAC) is a component of the CMEMS and its role is to ensure consistent and reliable access to a range of in situ data for service production and validation. For this purpose, CMEMS INSTAC collect multi-source/multiplatform data, and perform consistent quality control before distributing the data in a common format to the CMEMS Marine Forecasting Centres (MFC). The data can be found at http://www.marineinsitu.eu/. In this study, we considered all wave buoys moored in locations within 20km from a Sentinel-3A track and at a 1-km minimum distance to the coast. 70 buoys were selected, with distance to the coast comprised between 2 and 250 km. The locations of these buoys are shown on Figure 1.

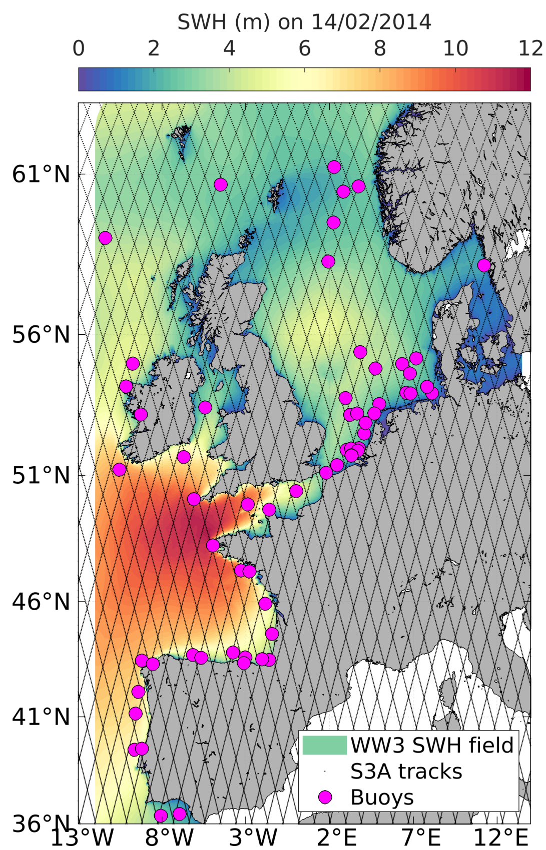

Figure 1: Location of the 70 wave buoys (magenta circles) moored within 20 km of Sentinel-3A ground tracks (dashed black lines) selected for this study. The background colorscale shows the SWH field from the high-resolution wave model during Ulla storm (February 14 2014).

2.3. High-resolution numerical wave model

The wave model hindcast used in this study is being developed at IFREMER in the context of the ResourceCODE project (OCEAN ERA-Net cofound) with the aim to provide accurate long-term sea state information for the exploitation of Marine Renewable Energy (https://resourcecode.ifremer.fr/). It is a regional implementation of the WAVEWATCH III (hereafter WW3) spectral wave model on a high-resolution unstructured mesh extending from the south of Spain to the Faroe Islands, and from the western Irish continental shelf to the Baltic Sea (-12°W to 13.5°E, 36°N to 63°N). The extension of the model grid is presented on Figure 1 with an example of simulated SWH field during Ulla storm on February, 14 2014. The hindcast covers a 28-year period, from 1993 to 2020. The bathymetry combines data from the EMODnet dataset (EMODnet 2016) and the HOMONIM dataset provided by the French Naval Hydrographic and Oceanographic Service (Shom) with a 0.001° resolution over the Channel and the Bay of Biscay. The spatial mesh contains 328,000 nodes and the resolution ranges from 10 km offshore to 200 m near the coast. The spectral grid consists of 36 directions and 36 exponentially spaced frequencies, from 0.0339Hz to 0.9526Hz. The physical parameterization corresponds to test T475, as described in Alday et al. (2021), which uses adjusted parameters for the wind-wave generation and swell dumping terms. The model is forced along its boundaries with wave spectra generated by a global WW3 wave model hindcast forced with ERA-5 hourly wind fields (Hersbach et al., 2020) and CMEMS-Globcurrent surface current fields (Global Ocean Multi Observation Product, MULTIOBS_GLO_PHY_REP_015_004). The regional model is forced by ERA-5 wind fields (with a bias correction for wind speeds larger than 21m/s), and with currents and water levels reconstructed from the MARS2D and FES2014 tidal harmonics database. Detailed information on the ResourceCODE model implementation and validation can be found in Accensi et al. (2021) and Alday et al. (2022). Moreover, implementation and validation of the global wave hindcast are described in Alday et al. (2021).

3. Methods

3.1. Buoy representativeness area

In order to characterize the spatial variability of the SWH in the vicinity of the buoy, and to quantify the spatial representativeness of the buoy SWH measurements, we implemented a methodology based on the results of the high resolution numerical wave hindcast described in Section 2.3, and inspired from the work of Nencioli and Quartly (2019). In this method, the time-series of simulated SWH at the buoy location is compared to the time-series of simulated SWH at every surrounding nodes located within a radius of 200km. The normalized bias (NBias) (systematic variability) and the scatter index (SI) (random variability) are computed between the buoy and its neighbouring nodes, to characterize both systematic and random variabilities, respectively. The NBias and SI values are then interpolated over a 200 x 200 km regular grid with 200m resolution in order to enhance the sampling in offshore regions, where the unstructured grid has a coarser resolution. The area presenting Nbias and SI values lower than 5% is then identified as the buoy representativeness area (BRA) and a polygon is fitted to encompass this area as closely as possible. The different steps of the methods are illustrated on Figure 2 for buoy 6200080, which is located nearby La Rochelle, on the west coast of France. Note that this method can be applied to other sea

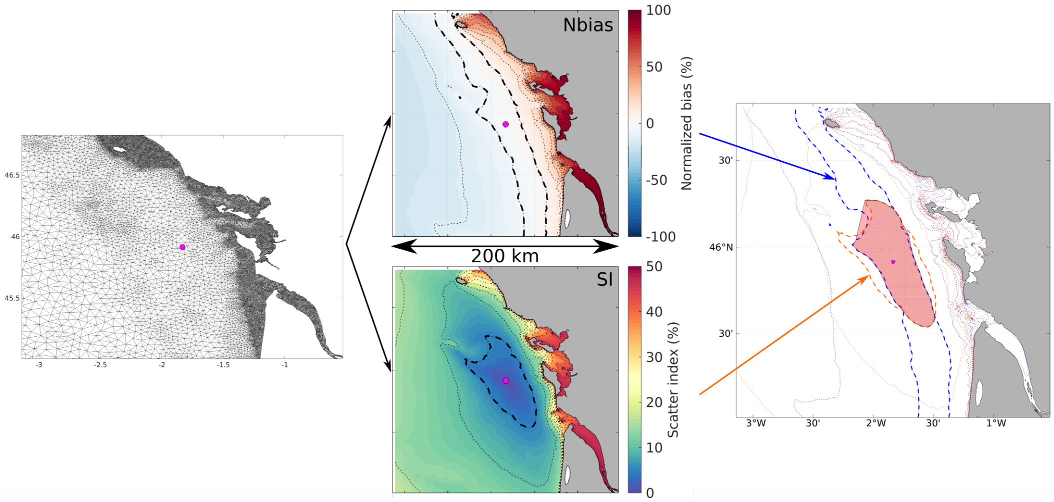

Figure 2: Processing of the buoy representativeness area for buoy 6200080 (nearby La Rochelle, France). Step1 (left panel): Differences between modelled SWH at buoy location and surrounding nodes are computed over the hindcast duration. Step2 (middle panel): Maps of normalized bias and scatter index are interpolated over 200kmx200km grid (tick black dashed lines indicate the 5% isocontour). Step3 (right panel): The intersection (dotted area) between areas with |Nbias| <5% (thick blue dashed line) and SI<5% (thick orange dashed line) is used to fit a convex polygon casting the buoy representativeness area (red shaded area).

state parameters, such as the wave period and direction as in Mureau et al. (2022), and other geophysical variables for which satellite-in situ collocation is required, for instance to investigate coastal sea level variability nearby tide gauges.

3.2. Data pairing methods

Data pairing methods (also known as collocation or matchup detection methods) are required to associate and compare values acquired by distinct measurement systems (model or sensor) at nearby location and time (e.g. satellite and in situ observations). Four data pairing methods are considered in this study. These methods are based on spatial criteria only since wave buoy measurements usually provide continuous hourly records, giving a maximum separation time between satellite and buoy records of 30min, which is sufficiently small to consider the sea state to be stationary. The four methods are:

1. The *static* method: it uses a fixed separation distance (radius) from the buoy location to sample all altimeter records within this distance. This method is used in most altimeter CAL/VAL studies based on in situ measurements. The selected threshold is usually 100km, but it can be relaxed to 300km in order to increase the number of available data pairs. Conversely, on the coastal zone this distance is often reduced but barely below 20km to keep a sufficient number of available data pairs. In this study we consider four separation distances : 100, 50, 20, and 5km.
2. The *polygon-based* method: it uses the polygon vertices derived from the buoy representativeness area analysis (see Section 3.1) to sample only the altimeter records within the area (polygon) of low sea state variability.
3. The *dynamic collocation* method: it uses model results dynamically (i.e. model results are analysed at the time of altimeter measurements)

to sample only the altimeter records for which modelled SWH difference between the buoy and the altimeter locations is below 5%, following Janssen et al. (2007).

4. The *dynamic correction* method: it uses the model results dynamically in order to correct the buoy measurement from the modelled SWH gradient between the buoy and the altmeter record location. In its original form, proposed by Jiang et al. (2022), this method gives the possibility to use several buoy data, with a weighting scheme based on the inverse squared distance, to characterize more precisely the sea state conditions at the altimeter record location. This method does not constrain the altimeter record sampling and can actually be used in combination with any of the method presented above. In our case we have considered the 50km static method to constrain the sampling.

Examples of sampling obtained with the static, polygon and dynamic collocation methods for buoy 6200192, nearby Nazaré in Portugal, are shown on Figure 3. Selected and rejected samples are shown as blue and black dots, respectively. For the static (left panel) and polygon (middle panel) methods, all altimeter records located within the sampling area (red shaded area) are selected, while for the dynamic collocation method (right panel), the sampling area varies at each satellite pass depending on the modelled SWH gradient. However, we see that with this latter method, altimeter records as far as 100km from the buoy can be selected.

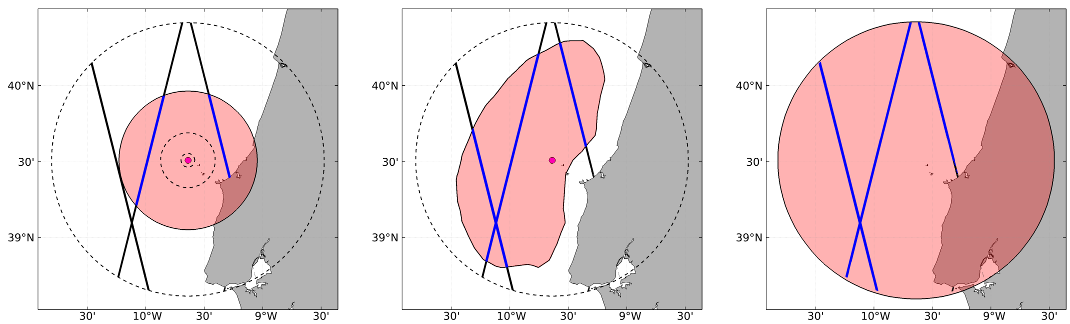

Figure 3: Examples of sampling regions (red shaded area) and altimeter records (blue dots) paired with buoy 6200192 (magenta circle) for the different data pairing methods. (left) the *static* method considers only measurements within a fixed separation distance (here 50km) from the buoy; four distances are considered: 100, 50, 20 and 5km (black circles) ; b) the *polygon-based* method considers only measurements occurring within the buoy representativeness area estimated from model hindcast ; c) the *dynamic collocation* method considers only measurements within 100km from the buoy for which modelled SWH difference between the buoy and the altimeter record is lower than 5%. Black dots represent altimeter records that are not selected for comparisons.

4. Results

4.1. Buoy representativeness areas

SWH representativeness areas were computed for the 70 buoys selected for this study from the analysis of the high resolution wave hindcast (see Section 2.3). These areas, shown on Figure 4, present strong heterogeneities in size and shape. In particular, offshore buoys are characterized by low and isotropic SWH variability resulting in large and near-circular representativeness areas with maximum surface areas of 9,000km^2 (i.e. with an equivalent radius of 55km), while nearshore buoys present very local error gradients resulting in reduced representativeness areas with surface areas as low as 7 km^2 (i.e. with an equivalent radius of 1.5km). Buoys at intermediate distance from the coast present significant cross-shore error gradients (not shown here) resulting in elongated (along-shore) representativeness areas. Although it is not the goal of this study to investigate which environmental factors controls the coastal sea state variability depicted by the buoy representativness area, we hypothesize that coastline geometry, and bathymetry, current and wind gradients are the main factors explaining coastal sea state variability, as investigated by many authors (e.g. Abdalla and Cavaleri, 2002; Ardhuin et al., 2012; Dodet et al., 2019a)

4.2. Sensitivity to data pairing methods

In Section 4.1 (Figure 4), we have shown that the choice of the data pairing method has a strong influence on the sampling of the altimeter records to be compared with the buoy measurements. This choice is therefore expected to impact the error metrics computed from these comparisons. In order to

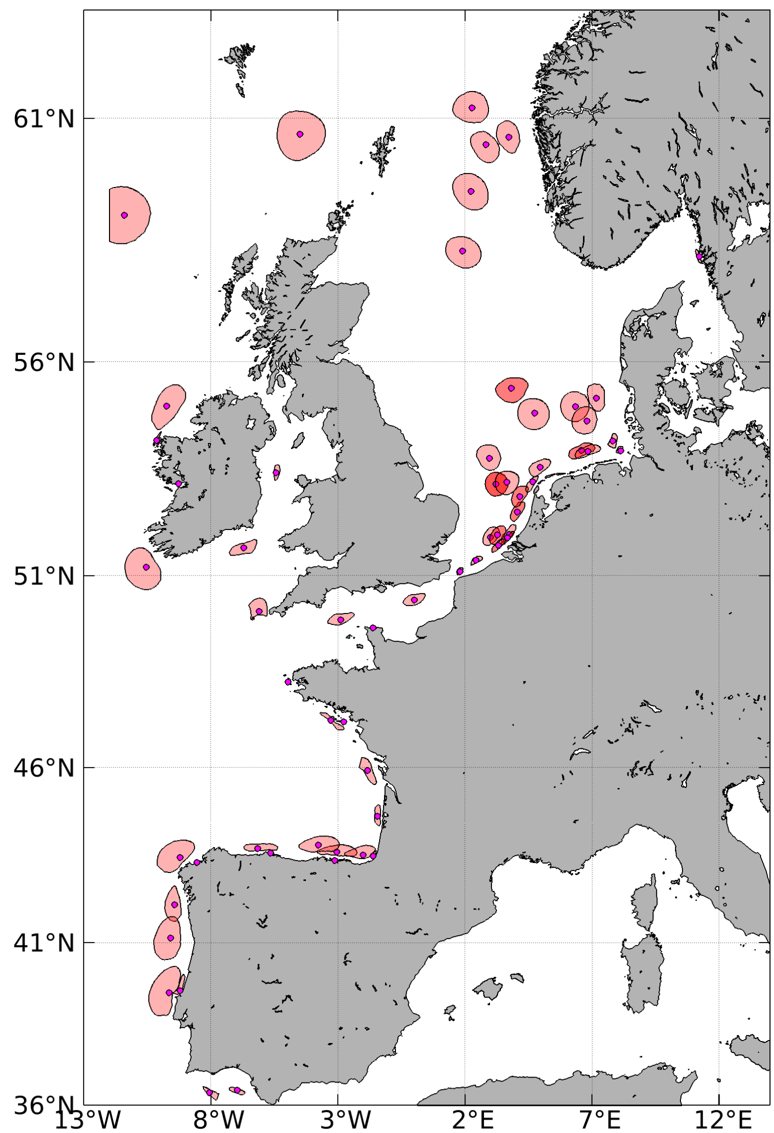

Figure 4: Map of the buoy representativeness area (BRA) polygons obtained for the 70 selected buoys.

investigate the sensitivity of altimeter validation results to the data pairing methods, we have compared Sentinel-3A SAR data and buoy data using data pairs given by the static, polygon, dynamic collocation and dynamic correction methods. For each method we computed the relative (with respect to the 100km-static method) number of data pairs ($Nval$), the normalized bias ($Nbias$), the scatter index (SI), and the correlation coefficient(R), as follows:

$$Nbias = \frac{\sum(A_i - B_i)}{\sum B_i} \tag{1}$$

$$SI = \sqrt{\frac{\sum[(A_i - \bar{A}_i) - (B_i - \bar{B}_i)]^2}{\sum B_i^2}} \tag{2}$$

$$R = \frac{\sum(A_i - \bar{A}_i)(B_i - \bar{B}_i)}{\sum(A_i - \bar{A}_i)^2 \sum(B_i - \bar{B}_i)^2} \tag{3}$$

where A_i and B_i are the altimeter and buoy records, respectively. Figure 5 compares the different metrics obtained with the four data pairing method, the first four bars corresponding to the four separation distances used with the static method (100km, 50km, 20km and 5km).

Looking at the relative number of data pairs ($Nval$) obtained with the static method, the first feature we note is the rapid decrease of available matchups when the maximum separation distance is reduced, with less than 5% sampled data with the 20km and 5km separation distances, matching the expected inverse square law of the footprint size. Conversely, the three model-based methods preserve between 10 to 35% of data, which is more comparable to the sampling obtained with the 20km-static method (28.5%). In terms of normalized bias, we see that $Nbias$ is systematically higher for the static method (6.9-8.8%) than for the model-based methods (3.6-5.4%). Same conclusions can be drawn for SI and R, for which the static method

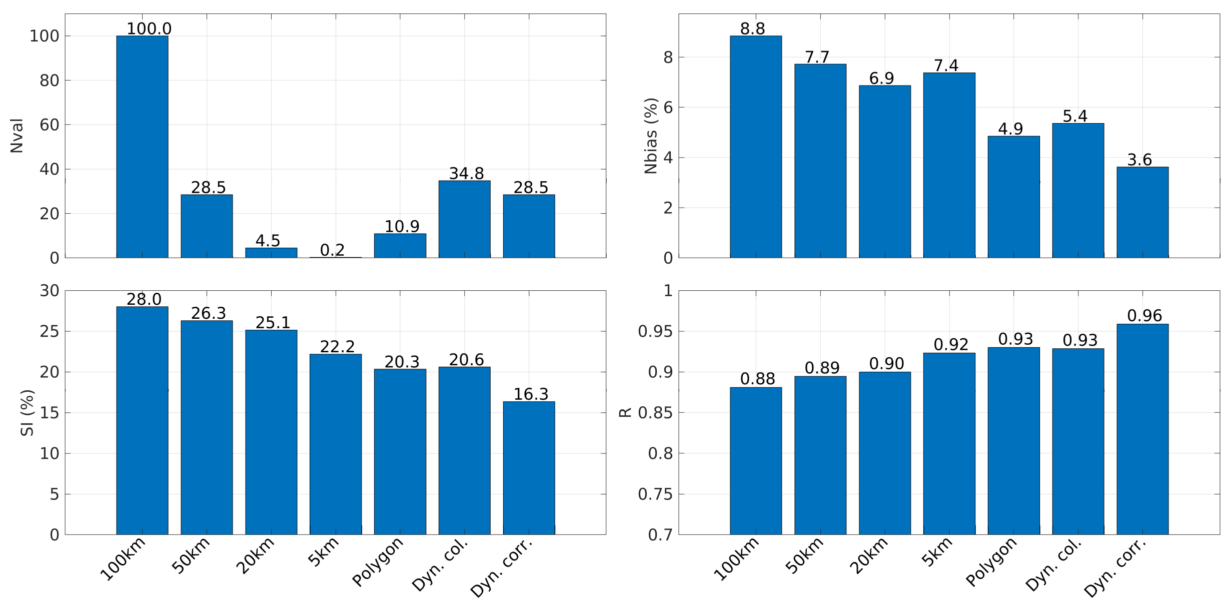

Figure 5: Relative number of data pairs ($Nval$), normalized bias ($Nbias$), scatter index (SI), and correlation coefficient(R) obtained from the comparisons between Sentinel 3A SAR and buoy SWH data for the different data pairing methods.

shows poorer performance (22.2-28.0% for SI and 0.88-0.92 for R) than for the model-based methods (16.3-22.2% for SI and 0.93-0.96 for R). Overall, the dynamic correction method gives the best score while preserving a significant amount of data (28.5%), slightly lower than the dynamic collocation method (34.8%). However, we may question whether this conclusion can be drawn for each buoy separately or only for the aggregated dataset. To answer this point, we estimated for each buoy which data pairing method provides the best score for the four considered parameters (Figure 6 and Table 1). For this analysis, we only considered the 50km separation distance for the static method, as it provides the best trade-off between the number of samples and the error metrics.

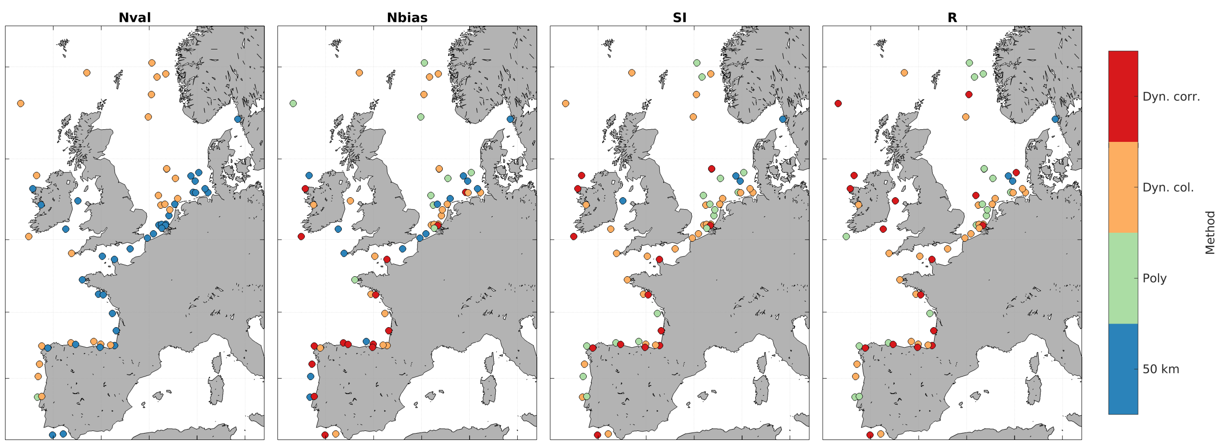

Figure 6: Spatial distribution of the data pairing methods providing the best score at each buoy location for the following metrics: relative number of data pairs ($Nval$), normalized bias ($Nbias$), scatter index (SI), and correlation coefficient(R) obtained from the comparisons between Sentinel 3A SAR and buoy SWH data.

First, we see that the maximum number of samples are either obtained with the 50km-static or the dynamic collocation methods (first panel). Note that the dynamic correction method uses the same sampling as the 50km-static method and therefore cannot be differentiated for this parameter (hence orange circles can be swapped with red circles). In terms of spatial distribution, we see that the 50km-static method provides the largest number of samples mostly for buoys located near the coast, while the dynamic collocation methods provides the largest number of samples for the offshore buoys. This can be explained by the fact that the dynamic collocation method considers all altimeter records within a 100km distance from the buoy for which the modelled SWH difference with the buoy location is small. In offshore conditions, a significant number of altimeter records located between 50-100km from the buoy must satisfy this condition, as opposed to nearshore conditions where SWH variability is much stronger. In terms of $Nbias$ we find that the dynamic collocation method gives the best score for the largest number of buoys (40%), while the polygon method gives the best score for the lowest number of buoys (16%). For SI and R, the three model-based methods are clearly better than the 50km-static method for most buoys, with the dynamic collocation method showing best scores for 44% and 40% of the buoys, respectively. These results contrast with the overall statistics presented on Figure 5 and using a dataset aggregating all buoy data, showing best scores with the dynamic correction method. This is certainly due to the different amount of data collected for each buoy, which induce different weighting on the results based on the aggregated dataset.

4.3. Evaluation of S3A coastal performance

In the previous section, we have shown that the use of a model-based data pairing methods to compare S3A and in situ data significantly reduced

Method	Nval (%)	Nbias (%)	SI (%)	R (%)
50km-static	57	21	6	4
Polygon	1	16	29	29
Dynamic collocation	41	40	44	40
Dynamic correction	57	23	21	27

Table 1: Percentage of buoys showing the best score for the following parameters: $Nval$, $Nbias$, SI, R (see also Figure 6). Note that the 50km-static and Dynamic correction methods share an equal number of values, hence a similar ranking for this parameter.

the spatial representativeness errors induced by the strong SWH spatial variability in the vicinity of the coastal buoys. The overall performance of S3A (SAR) SWH measurements are therefore estimated with lower uncertainties thanks to these methods. In this last Section, we will examine the systematic and random errors of S3A SWH measurements as a function of the distance to the coast, considering three S3A products: PLRM, SAR and LR-RMC.

Figure 7 shows the normalized bias and the scatter index between S3A (PLRM, SAR and LR-RMC) and in situ data for each buoy as a function of the distance between the buoy and the nearest coastline. First, we see that most (67%) of the European buoys are located within 50 km from the coast, and the furthest offshore buoys (namely A121 and A122 amidst the North Sea) are moored as far as 240km from the coast. The circle's colors indicate the mean SWH at the associated buoy, which varies between 0.8m and 3.6m. The first striking pattern common to all S3A products is the increased error towards the coast. More specifically, the range of the normalized bias increases from [-2 ; 20]% in the 50-250km coastal strip to [-5 ; 95]% in the 2-50km coastal strip. Likewise, the range of SI increases from [11 ; 25]%

in the 50-250km coastal strip to [10 ; 100]% in the 2-50km coastal strip. Moreover, the systematic error is positive for a large majority of the buoys, indicating an overestimate of S3A SWH data wrt. buoy data, which is particularly pronounced near the coast. Several factors may explain this tendency: first, radar altimeter SWH measurements often present bias of the order of 5-10% that require *a posteriori* calibration against in situ measurements or reference altimeter missions (see for instance Zieger et al., 2009; Dodet et al., 2020); second, the sampling pattern of altimeter data collocated with coastal buoys is often skewed offshore (wrt buoy position) because a higher fraction of altimeter data is flagged as invalid near the coast. Given that coastal sea states attenuate towards the coast (e.g. Passaro et al., 2021), there is a dominance of higher-than-average altimeter SWH in the selected samples, as explained by Jiang et al. (2022); last, radar altimeter sensors do not have a sufficient resolution (around 50cm for Ku-band instruments) to resolve low sea states, which often results in increased error level near the coast where sea states are lower on average. This is particularly visible from Figure 7, where the buoys presenting the lowest average SWH (dark blue circles) present the largest errors. If we now compare the different products, we can see the clear improvement of SAR and LR-RMC data compared to the PLRM data. The mean normalized bias decreases from 18.6% (PLRM) to 5.6% (LR-RMC) and the mean SI decreases from 45.7% (PLRM) to 20% (LR-RMC). On average, the LR-RMC processing presents the best performance, with a reduction of the error of approximately 20% with respect to SAR data.

In order to extend the S3a performance analysis with an additional reference data source and to reduce the impact of the buoy location with re-

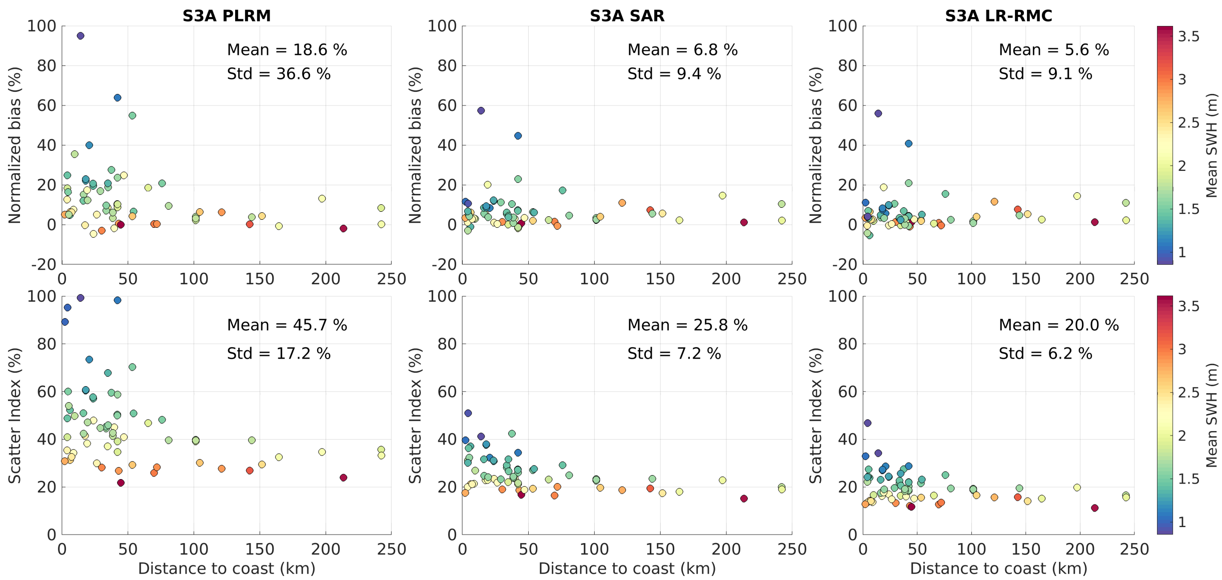

Figure 7: Nbias (upper panels) and SI (lower panels) computed from the differences between S3A PLRM (left panels), SAR (middle panels) and LR-RMC (right panels) and buoy SWH data at each buoy as a function of the distance of the buoy to the coast. Colorscale indicates the mean SWH at the location of each buoy.

spect to the altimeter ground tracks, the SWH data simulated with the high-resolution wave model were interpolated at the altimeter record positions, and error metrics were binned as a function of the distance to the coast, using bins of 5-km width from 0 to 300km (Figure 8). Here again, we see that the errors increase towards the coast, and that the normalized bias is mostly positive (around 5%) for all products. Yet, in comparison to the in situ data analysis (Figure 7), the bias increase occurs closer to the coast, at around 40km for PLRM and 20 km for SAR data. For LR-RMC the bias remains very stable (between 0-10%) up to 1km from the coast (see zoom over the 0-20km coastal strip on the left panels). For SI, we see that the error starts increasing at around 70km for PLRM data. For SAR data SI presents a sharp increases at around 7km from the coast. And here again, LR-RMC data remains very stable (between 10-22%) up to 1km from the coast. Finally, the correlation coefficient R confirm the previous tendencies, with decreasing values at around 70km for PLRM data, a sharp decrease at around 10km for SAR data, and a much more stable trend (above 0.9) for LR-RMC data. If we compare the three products, we see that the biases are very similar (even slightly lower for PLRM) in the 50-300km region, while they become much lower for SAR and LR-RMC data in the 0-50km region. For SI and R, there is a large gap between PLRM error level on one side, and SAR and LR-RMC error level on the other side. Moreover, the LR-RMC data give the best scores in both offshore and nearshore waters, confirming the excellent performance of the LR-RMC processing method. In the 0-20km region, the average scores for LR-RMC are : NBias = 2.4%, SI = 18.9% and R = 0.95. In order to further investigate the differences between the products, the number of valid values was also binned as a function of the distance to the coast. While these numbers are fairly similar between products up to 7km from the coast, we can see that it drops more rapidly for LR-RMC in the 1-7km region. This reflects the different data editing information provided for each product which are more or less stringent in the coastal zone. With the LR-RMC product, this information seems to be particularly efficient to reject invalid altimeter record in the coastal zone, as also evidenced by Schlembach et al. (2020), which likely contributes to the improved performance compared to the SAR data.

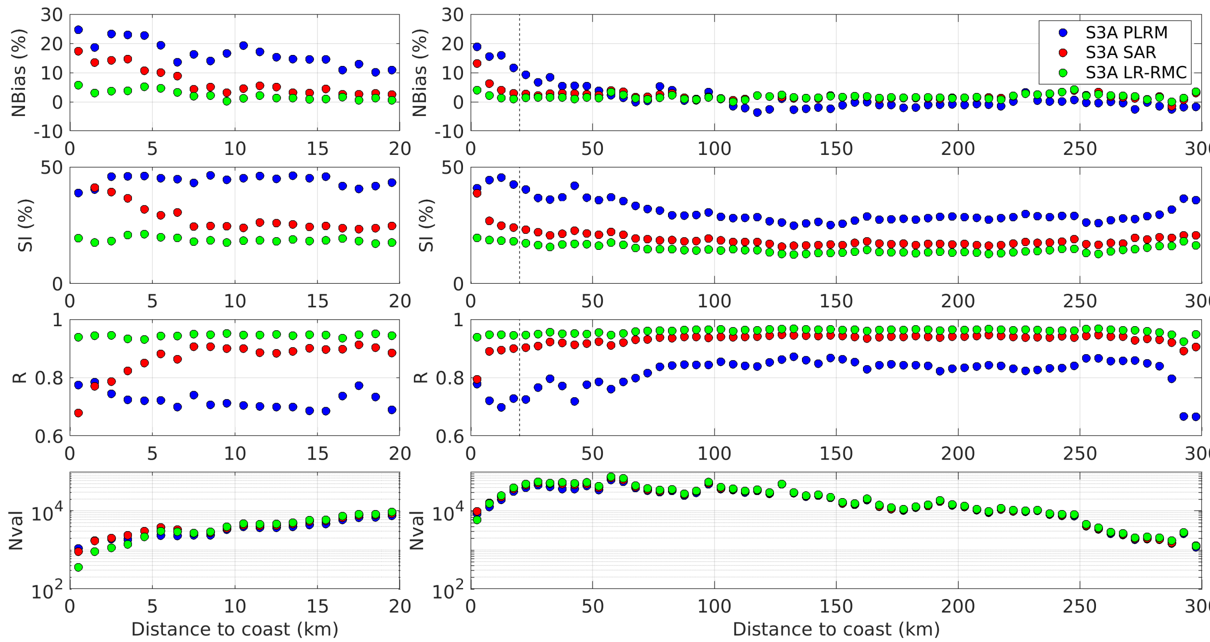

Figure 8: Nbias (top-row panels), SI (second-row panels), R (third-row panels) and number of valid values NVal (bottom-row panels) computed from the differences between S3A PLRM (blue circles), SAR (red circles) and LR-RMC (green circles) and model SWH data as a function of the distance of the altimeter record to the coast, with bins of 10-km width. Left panels correspond to a zoom over the 0-20km from the coast, using bins of 1-km width.

5. Conclusion

Sea state variability is known to be strongly enhanced in the coastal zone due to interactions between waves, currents, winds, bathymetry and coastline geometry. In Section 4.1, we have used a high-resolution wave hindcast in order to estimate the spatial scales over which the SWH measured by European coastal buoys can be considered homogeneous (in a statistical sense). Our results show that these so-called buoy representativeness areas vary strongly in size and shape, depending on the buoy environmental settings, and can be as small as an equivalent disk's radius of 1.5km (see Figure 2). Knowing that the conventional data pairing (or collocation) methods used to compare altimeter and in situ data in deep water usually assumes sea state homogeneity over 50 to 100 km, it is clear that such methods cannot be directly applied for the validation of coastal altimeter SWH data without impairing the results. To demonstrate it, we computed in Section 3.2 statistical error metrics (e.g. normalized bias, scatter index) over samples obtained with several data pairing methods, accounting or not for sea state variability, for comparing S3A and in situ SWH in the coastal zone. Our results confirm the efficiency of model-based data pairing methods to reduce spatial representativeness errors related to coastal sea state variability, while preserving a sufficient large sample from the population. For instance, in comparison to the 50-km static collocation method, the dynamic collocation method gives a Nbias 30% lower and a SI 22% lower for a sampling size 22% larger (see Figure 5). Having improved our confidence of the comparisons between altimeter and in situ data in the coastal zone, we evaluated the coastal performance of three S3A products, using different acquisition mode and processing methods, namely the

PLRM, the SAR and the LR-RMC products (Section 4.3). Our results show that all three products present increased error levels in the 0-50km region, which can partly be attributed to the lower sea state conditions affecting some of the coastal buoys that are badly measured by Ku-band altimeter sensors. Ignoring these buoys strongly reduces the range of error levels in the 0-50km region, particularly for the SAR and LR-RMC data (see Figure 7). These results are confirmed by comparing the altimeter SWH measurements with simulated SWH from the high-resolution model, which allows to access SWH measurements along the altimeter tracks and, therefore, reduce the impact of asymmetric sampling patterns and increase the sample size. These comparisons clearly show the improved performance of SAR and LR-RMC products compared to PLRM, in both offshore and coastal waters (see Figure 8). They also reveal the consistency of the S3A LR-RMC measurements up to 1km from the coast partially due to an efficient data editing procedure, which results in stable error metrics over the 0-20km region, with average NBias = 2.4%, SI = 18.9% and R = 0.95.

6. Acknowledgments

This research is funded by the European Space Agency through the Sea State CCI project of the Climate Change Initiative (CCI) (ESA ESRIN, Contract 4000123651/18/I-NB).

References

Abdalla, S., Cavaleri, L., 2002. Effect of wind variability and variable air density on wave modeling. Journal of Geophysical Research: Oceans 107, 17–1–17–17. URL: https://onlinelibrary.wiley.com/doi/abs/10.1029/2000JC000639, doi:10.1029/2000JC000639. _eprint: https://onlinelibrary.wiley.com/doi/pdf/10.1029/2000JC000

Accensi, M., Alday Gonzalez, M.F., Maisondieu, C., Raillard, N., Darbynian, D., Old, C., Sellar, B., Thilleul, O., Perignon, Y., Payne, G., O'Boyle, L., Fernandez, L., Dias, F., Chumbinho, R., Guitton, G., 2021. ResourceCODE framework: A high-resolution wave parameter dataset for the European Shelf and analysis toolbox, in: EWTEC 2021, Plymouth, UK. URL: https://archimer.ifremer.fr/doc/00736/84812/.

Alday, M., Accensi, M., Ardhuin, F., Dodet, G., 2021. A global wave parameter database for geophysical applications. Part 3: Improved forcing and spectral resolution. Ocean Modelling 166, 101848. URL: https://www.sciencedirect.com/science/article/pii/S1463500321001001, doi:10.1016/j.ocemod.2021.101848.

Alday, M., Ardhuin, F., Dodet, G., Accensi, M., 2022. Accuracy of numerical wave model results: Application to the Atlantic coasts of Europe. EGUsphere , 1–39URL: https://egusphere.copernicus.org/preprints/2022/egusphere-2022-481/, doi:10.5194/egusphere-2022-481. publisher: Copernicus GmbH.

Ardhuin, F., Roland, A., Dumas, F., Bennis, A.C., Sentchev, A., Forget, P., Wolf, J., Girard, F., Osuna, P., Benoit, M., 2012. Numerical Wave Modeling in Conditions with Strong Currents: Dissipation, Refraction, and Relative Wind. Journal of Physical Oceanography 42, 2101–2120. URL: http://journals.ametsoc.org/doi/abs/10.1175/JPO-D-11-0220.1, doi:10.1175/JPO-D-11-0220.1.

Ardhuin, F., Stopa, J.E., Chapron, B., Collard, F., Husson, R., Jensen, R.E., Johannessen, J., Mouche, A., Passaro, M., Quartly, G.D., Swail, V., Young, I., 2019. Observing Sea States. Frontiers in Marine Science 6. URL: https://www.frontiersin.org/articles/10.3389/fmars.2019.00124/full, doi:10.3389/fmars.2019.00124.

Boy, F., Desjonqueres, J.D., Picot, N., Moreau, T., Raynal, M., 2017. CryoSat-2 SAR-Mode over Oceans: Processing Methods, Global Assessment, and Benefits. IEEE Transactions on Geoscience and Remote Sensing 55, 148–158. doi:10.1109/TGRS.2016.2601958.

Chelton, D.B., Walsh, E.J., MacArthur, J.L., 1989. Pulse Compression and Sea Level Tracking in Satellite Altimetry. Journal of Atmospheric and Oceanic Technology 6, 407–438. doi:10.1175/1520-0426(1989)006¡0407:PCASLT¿2.0.CO;2.

Dodet, G., Bertin, X., Bouchette, F., Gravelle, M., Testut, L., Wöppelmann, G., 2019a. Characterization of Sea-level Variations Along the Metropolitan Coasts of France: Waves, Tides, Storm Surges and Long-term Changes. Journal of Coastal Research 88, 10–24. URL: https://bioone.org/journals/Journal-of-Coastal-Research/volume-88/issue-sp1/SI88 doi:10.2112/SI88-003.1.

Dodet, G., Melet, A., Ardhuin, F., Bertin, X., Idier, D., Almar, R., 2019b. The Contribution of Wind-Generated Waves to Coastal Sea-Level Changes. Surveys in Geophysics URL: https://doi.org/10.1007/s10712-019-09557-5, doi:10.1007/s10712-019-09557-5.

Dodet, G., Piolle, J.F., Quilfen, Y., Abdalla, S., Accensi, M., Ardhuin, F., Ash, E., Bidlot, J.R., Gommenginger, C., Marechal, G., Passaro, M., Quartly, G., Stopa, J., Timmermans, B., Young, I., Cipollini, P., Donlon, C., 2020. The Sea State CCI dataset v1: towards a sea state climate data record based on satellite observations. Earth System Science Data 12, 1929–1951. URL: https://essd.copernicus.org/articles/12/1929/2020/, doi:https://doi.org/10.5194/essd-12-1929-2020. publisher: Copernicus GmbH.

Hersbach, H., Bell, B., Berrisford, P., Hirahara, S., Horányi, A., Muñoz-Sabater, J., Nicolas, J., Peubey, C., Radu, R., Schepers, D., Simmons, A., Soci, C., Abdalla, S., Abellan, X., Balsamo, G., Bechtold, P., Biavati, G., Bidlot, J., Bonavita, M., Chiara, G.D., Dahlgren, P., Dee, D., Diamantakis, M., Dragani, R., Flemming, J., Forbes, R., Fuentes, M., Geer, A., Haimberger, L., Healy, S., Hogan, R.J., Hólm, E., Janisková, M., Keeley, S., Laloyaux, P., Lopez, P., Lupu, C., Radnoti, G., Rosnay, P.d., Rozum, I., Vamborg, F., Villaume, S., Thépaut, J.N., 2020. The ERA5 global reanalysis. Quarterly Journal of the Royal Meteorological Society 146, 1999–2049. URL:

https://rmets.onlinelibrary.wiley.com/doi/abs/10.1002/qj.3803, doi:10.1002/qj.3803. _eprint: https://rmets.onlinelibrary.wiley.com/doi/pdf/10.1002/qj.3803.

Hithin, N.K., Remya, P.G., Balakrishnan Nair, T.M., Harikumar, R., Kumar, R., Nayak, S., 2015. Validation and Intercomparison of SARAL/AltiKa and PISTACH-Derived Coastal Wave Heights Using In-Situ Measurements. IEEE Journal of Selected Topics in Applied Earth Observations and Remote Sensing 8, 4120–4129. doi:10.1109/JSTARS.2015.2418251. conference Name: IEEE Journal of Selected Topics in Applied Earth Observations and Remote Sensing.

Jackson, F.C., 1979. The reflection of impulses from a nonlinear random sea. Journal of Geophysical Research: Oceans 84, 4939–4943. URL: https://onlinelibrary.wiley.com/doi/abs/10.1029/JC084iC08p04939, doi:10.1029/JC084iC08p04939.

Janssen, P.A.E.M., Abdalla, S., Hersbach, H., Bidlot, J.R., 2007. Error Estimation of Buoy, Satellite, and Model Wave Height Data. Journal of Atmospheric and Oceanic Technology 24, 1665–1677. URL: https://journals.ametsoc.org/jtech/article/24/9/1665/2940/Error-Estimation-of-Bu doi:10.1175/JTECH2069.1. publisher: American Meteorological Society.

Jiang, H., Fu, G., Ren, L., 2022. Evaluation of Coastal Altimeter Wave Height Observations Using Dynamic Collocation. IEEE Transactions on Geoscience and Remote Sensing 60, 1–8. doi:10.1109/TGRS.2022.3198430. conference Name: IEEE Transactions on Geoscience and Remote Sensing.

Moreau, T., Cadier, E., Boy, F., Aublanc, J., Rieu, P., Raynal, M., Labroue, S., Thibaut, P., Dibarboure, G., Picot, N., Phalippou, L., Demeestere, F., Borde, F., Mavrocordatos, C., 2021. High-performance altimeter Doppler processing for measuring sea level height under varying sea state conditions. Advances in Space Research 67, 1870–1886. URL: https://www.sciencedirect.com/science/article/pii/S027311772030911X, doi:10.1016/j.asr.2020.12.038.

Moreau, T., Tran, N., Aublanc, J., Tison, C., Le Gac, S., Boy, F., 2018. Impact of long ocean waves on wave height retrieval from SAR altimetry data. Advances in Space Research 62, 1434–1444. URL: https://www.sciencedirect.com/science/article/pii/S0273117718304708, doi:10.1016/j.asr.2018.06.004.

Mureau, G., Dodet, G., Suanez, S., 2022. Characterizing sea state variability along the French Atlantic coast. Proceedings of the XVIIèmes Journées Nationales Génie Côtier – Génie Civil , 129–142doi:10.5150/jngcgc.2022.015.

Nencioli, F., Quartly, G.D., 2019. Evaluation of Sentinel-3A Wave Height Observations Near the Coast of Southwest England. Remote Sensing 11, 2998. URL: https://www.mdpi.com/2072-4292/11/24/2998, doi:10.3390/rs11242998. number: 24 Publisher: Multidisciplinary Digital Publishing Institute.

Passaro, M., Hemer, M.A., Quartly, G.D., Schwatke, C., Dettmering, D., Seitz, F., 2021. Global coastal attenuation of wind-waves observed with radar altimetry. Nature Communications 12, 3812. URL: https://www.nature.com/articles/s41467-021-23982-4, doi:10.1038/s41467-021-23982-4.

Passaro, M., Rose, S.K., Andersen, O.B., Boergens, E., Calafat, F.M., Dettmering, D., Benveniste, J., 2018. ALES+: Adapting a homogenous ocean retracker for satellite altimetry to sea ice leads, coastal and inland waters. Remote Sensing of Environment 211, 456–471. URL: http://www.sciencedirect.com/science/article/pii/S0034425718300920, doi:10.1016/j.rse.2018.02.074.

Quilfen, Y., Chapron, B., 2020. On denoising satellite altimeter measurements for high-resolution geophysical signal analysis. Advances in Space Research URL: http://www.sciencedirect.com/science/article/pii/S0273117720300235, doi:10.1016/j.asr.2020.01.005.

Raney, R., 1998. The delay/Doppler radar altimeter. IEEE Transactions on Geoscience and Remote Sensing 36, 1578–1588. doi:10.1109/36.718861. conference Name: IEEE Transactions on Geoscience and Remote Sensing.

Schlembach, F., Passaro, M., Quartly, G.D., Kurekin, A., Nencioli, F., Dodet, G., Piollé, J.F., Ardhuin, F., Bidlot, J., Schwatke, C., Seitz, F., Cipollini, P., Donlon, C., 2020. Round Robin Assessment of Radar Altimeter Low Resolution Mode and Delay-Doppler Retracking Algorithms for Significant Wave Height. Remote Sensing 12, 1254. URL: https://www.mdpi.com/2072-4292/12/8/1254, doi:10.3390/rs12081254. number: 8 Publisher: Multidisciplinary Digital Publishing Institute.

Serafin, K.A., Ruggiero, P., Stockdon, H.F., 2017. The relative contribution of waves, tides, and nontidal residuals to extreme total water levels on U.S. West Coast sandy beaches. Geophysical Research Letters 44, 1839–1847. URL: https://agupubs.onlinelibrary.wiley.com/doi/abs/10.1002/2016GL071020, doi:10.1002/2016GL071020.

Tourain, C., Piras, F., Ollivier, A., Hauser, D., Poisson, J.C., Boy, F., Thibaut, P., Hermozo, L., Tison, C., 2021. Benefits of the Adaptive Algorithm for Retracking Altimeter Nadir Echoes: Results From Simulations and CFOSAT/SWIM Observations. IEEE Transactions on Geoscience and Remote Sensing , 1–14doi:10.1109/TGRS.2021.3064236. conference Name: IEEE Transactions on Geoscience and Remote Sensing.

Vignudelli, S., Birol, F., Benveniste, J., Fu, L.L., Picot, N., Raynal, M., Roinard, H., 2019. Satellite Altimetry Measurements of Sea Level in the Coastal Zone. Surveys in Geophysics 40, 1319–1349. URL: https://doi.org/10.1007/s10712-019-09569-1, doi:10.1007/s10712-019-09569-1.

Yaplee, B.S., Shapiro, A., Hammond, D.L., Au, B.D., Uliana, E.A., 1971. Nanosecond Radar Observations of the Ocean Surface from a Stable Platform. IEEE Transactions on Geoscience Electronics 9, 170–174. doi:10.1109/TGE.1971.271490. conference Name: IEEE Transactions on Geoscience Electronics.

Zieger, S., Vinoth, J., Young, I.R., 2009. Joint Calibration of Multiplatform Altimeter Measurements of Wind Speed and Wave Height over the Past 20 Years. Journal of Atmospheric and Oceanic Technology 26, 2549–2564. URL:

https://journals.ametsoc.org/doi/10.1175/2009JTECHA1303.1,
doi:10.1175/2009JTECHA1303.1.